Unraveling the role of feed temperature and cross-flow velocity on organic fouling in membrane distillation using response surface methodology

Unraveling the role of feed temperature and cross-flow velocity on organic fouling in membrane distillation using response surface methodology

Francesco Ricceri[a], Bastiaan Blankert [b], Johannes S. Vrouwenvelder[b], Alberto Tiraferri[a]*, Luca Fortunato[b]*

[a] Department of Environment, Land and Infrastructure Engineering (DIATI), Politecnico di Torino, Corso Duca degli Abruzzi 24, Turin, 10129, Italy

[b] Water Desalination and Reuse Center (WDRC), King Abdullah University of Science and Technology (KAUST), Biological & Environmental Science & Engineering Division (BESE), Thuwal 23955-6900, Saudi Arabia

* Corresponding authors

Highlights

- Feed temperature governs the fouling behaviour more than cross-flow velocity
- Higher feed temperature increases the fouling accumulation
- Higher cross-flow velocity decreases the fouling accumulation
- Feed temperature and cross-flow velocity were statistically significant for the RSM
- RSM is a powerful tool to assess performance and fouling behaviour in MD

Abstract

Understanding the role of operating condition on fouling development in membrane distillation (MD) is critical for the further optimization of MD technology. In this study, organic fouling development in MD was investigated with a synthetic model solution of humic acid varying the feed inlet temperature from 35 to 65 °C and the cross-flow velocity from 0.21 to 0.42 m/s. For each experiment, the final fouling layer thickness was estimated using optical coherence tomography, a non-invasive imaging technique. The set of experiments was mined to model the initial flux decline, the final flux, and the final foulant thickness responses by central composite design, a useful response surface methodology (RSM) tool. A strong influence on the initial flux was observed by varying feed inlet temperature. The results indicated a linear increment of the fouling thickness by increasing the feed inlet temperatures. Overall, the feed inlet temperature governed both the initial flux decline and the fouling deposition rate. A more complex behaviour was observed by varying the cross-flow velocity. To this extent, higher cross-flow velocities showed a positive effect on the initial flux, which however translated in larger values of the initial flux decline rate. On the other hand, the higher shear stress contributed to a decrease of the final fouling layer thickness. The proposed approach was proven to be a valuable tool to assess the role of the operating conditions on fouling and process performance in MD.

Keywords: Direct contact membrane distillation (DCMD); Membrane fouling; Optical coherence tomography (OCT); Response surface methodology (RSM);

1 Introduction

Membrane distillation is a thermal-based desalination technology which has gained an exponential interest during the last decades [1, 2]. Among all the possible membrane distillation configurations, direct contact membrane distillation (DCMD) is the most compact. Due to its simplicity, this process has been extensively studied at laboratory scale to approach scale-up applications in MD [3-5]. In fact, DCMD does not require an external condenser and it is more suitable for water-based applications than air gap, vacuum, or sweep gas membrane distillation. In DCMD, the hot feed and the cold permeate solutions are in contact with a hydrophobic membrane. Under ideal working conditions, only water vapor passage is allowed through this microporous membrane [6, 7]. However, several operational challenges might cause decrease in productivity or even process failure [8]. According to the type of treated feed solution, three main drawbacks observed in the operational DCMD phase are: (i) pore wetting, (ii) mineral scaling, and (iii) membrane fouling. Wetting mainly occurs when membrane hydrophobicity is reduced, together with the liquid entry pressure, to the point which allows liquid passage through the pores [9, 10]. Wetting is easily induced by amphiphilic molecules, such as surfactants, and it leads to process failure even in a preliminary recovery stage [11, 12]. Mineral scaling is due to crystal formation of salts at the solid membrane interface, initiating a rapid and severe flux decline which can also translate into pore wetting and membrane damage [13]. Membrane fouling leads to flux reduction over time due by accumulation of feed contaminants on the membrane surface [14].

With the increasing interest in MD, the number of possible applications has been also expanded. As a thermal-based process, MD has been largely used for desalination to produce high-quality water while concentrating the feed above typical reverse osmosis limits [15]. Recently, DCMD

has been also employed for the treatment of challenging wastewater, such as produced water, textile, and pharmaceutical wastewater [16-18]. Within this range of possible applications, recent studies demonstrated how effective pre-treatment strategies and process optimization could highly reduce pore-wetting and mineral scaling propensity [16, 19]. In this context, membrane fouling is still considered one of the main bottlenecks of MD operations [20, 21]. Among different foulant species, humic substances showed particularly high fouling propensity in low-pressure processes due to high adhesion capacity of these compounds on the membranes [22]. Humic acids are also the major constituents of natural organic matter, as well as widely present constituents in surface water, groundwater, and seawater [23]. In this study, organic fouling in DCMD was investigated by using humic acid as model compound under accelerated fouling conditions.

Optical coherence tomography (OCT) has been recently demonstrated as an effective and versatile tool for fouling characterization. This non-destructive technique enables monitoring the filtration system under continuous operation, providing real-time information of the fouling layer [24, 25]. OCT allows acquiring non-invasively 2D cross-sectional and 3D volumetric images with micron-level resolution without interfering with the membrane operation. Recently, the use of OCT has been employed for studying the fouling behavior in MD when treating textile, pharmaceutical wastewater, and concentrated brines [17, 18, 26]. In these studies, OCT results were efficiently linked to process performance data allowing an in-depth understanding on how fouling and scaling impact the water flux during the DCMD process. However, these literature studies were often limited to narrow ranges of operative conditions in MD. To extend the understanding of fouling under a wider range of temperatures and cross-flow velocities, response surface modeling (RSM) was implemented in this study through Design Expert software [27-29].

One of the way to implement RSM is by using central composite design (CCD), an array whereby investigated parameters are efficiently distributed to allow a second-order generalized regression between the experimental results [30, 31]. Recently, RSM combined with CCD has gained a growing interest in membrane process optimization as it is able to consider several variables at the same time with easy evaluation of the generated responses. An interesting application of RSM in MD was developed by Shokrollahi et al., who effectively modeled flux and thermal efficiency for a wide range of interacting parameters [32]. There, numerical modeling with CCD method for flux optimization showed that temperature and module length have the most important influence on MD productivity.

In this study, central composite design is implemented to guide the design of MD experiments conducted with different combinations of feed inlet temperature and cross-flow velocity. The experiments are performed with a synthetic model solution of humic acid, where the distillate flux is monitored as a function feed volume concentration factor. Additionally, OCT *in-situ* monitoring is employed to characterize the fouling layer developed at the end of each MD test. The flux performance and fouling data are discussed and critically examined also to assess a valuable experimental based modeling. Therefore, (i) the initial flux decline rate, (ii) the final flux, (iii) the total flux decline, and (iv) the final fouling thickness are applied as responses (dependent variables) in the RSM analysis to investigate the mechanism of fouling and to identify the most suitable DCMD operating conditions. The investigation assesses the role of process parameters and governing factors on fouling in MD, and it proposes the rational deployment of RSM as a tool to move toward scale-up applications.

2 Materials and Methods

2.1 Membrane and Feed composition

Accelerated fouling conditions were employed in this study using a synthetic feed solution with an initial humic acid (HA) concentration of 500 mg/L in deionized (DI) water. To enhance the fouling deposition, 20 mM of calcium chloride, $CaCl_2$, was also added to the feed solution [33]. HA and $CaCl_2$ were purchased from Sigma-Aldrich. The organic compound was received in powder form. The stock solution was prepared by dissolving the chemicals in 600 mL of DI water. The stock was then added, prior to flux stabilization, to the remaining 400 mL of deionized water used as initial feed. Initial volumes of 1 L were thus used for both the feed and permeate solutions, the latter consisting of DI water.

A commercially available hydrophobic polytetrafluoroethylene with a polypropylene support (PP-PTFE) membrane (Membrane Solutions corp., US) was used for all the experiments. The membrane characteristics, provided by the manufacturer or obtained in the lab, are listed in Table 1. The membrane permeability coefficient was calculated by dividing the experimental water flux by the vapor pressure difference across the membrane (see calculated angular coefficient from Fig S.1).

Table 1. Porous PP-PTFE membrane characteristics

Data source	Parameter	Units	Value
Provided by the manufacturer	Thickness	μm	174 - 245
	Mean pore size	μm	0.22
	Bubble point	psi	16.0-20.3
From experiments	Membrane permeability coefficient	kg $m^{-2}h^{-1}bar^{-1}$	143.8

2.2 MD lab setups

All the MD tests were performed in direct contact membrane distillation (DCMD) configuration with a lab-scale batch system. In this process, the feed and permeate streams were circulated counter-currently on their respective sides of the hydrophobic membrane, not enabling liquid passage through the pores. Thanks to the applied thermal gradient, the colder liquid is enriched by the water vapor extracted from the feed stream during the process. Ranges of feed temperature of 35 - 65 °C and feed cross-flow velocity of 0.21 - 0.42 m/s (deriving from a cross-flow rate ranging from 25 to 50 L/h) were investigated in this study. To clearly assess the role of feed parameters on fouling deposition, a constant temperature and cross-flow velocity of 20 °C and 0.1 m/s were maintained in the permeate side. For the same reason, no feed spacer was used. The temperatures in the feed and permeate inlet of the flow cell were maintained constant throughout the experiment using a thermostatic water bath and a chiller (Corio-CD, Julabo, Germany). The heat exchangers were accurately controlled by the temperature sensors integrated in the conductivity meters (TetraCon 325, Xylem Analytics, Germany) located just before the inlet of the flow cell. On the permeate side, purified water with electrical conductivity below 20 µS/cm was used, whereas the initial feed conductivity was 4.2 ± 0.2 mS/cm. For each experiment, the permeate conductivity was continuously monitored to ensure no liquid passage during the tests, i.e., no pore wetting. Cross-flow velocity and outlet-temperature were measured by digital cross-flow meters located in proximity of the flow cell outlet. The flux across the membrane was calculated by recording the change in weight of the permeate tank in time through a computer-interfaced balance. All the instruments were digitally connected and controlled by Lab View software. The DCMD flow cell in polymethyl methacrylate was

customized to allow *in-situ* characterization with OCT. The flow cell was had dimensions of 10.0 × 3.3 × 0.1 cm (length × width × height) for a total active membrane area of 33 cm^2.

2.3 Design of experiments and statistical analysis

Design Expert software was used to setup and analyze the response surface methodology (RSM) for DCMD experiments. Central composite design (CCD) was applied to define the number of runs needed for the optimization of the variables and responses. Feed inlet temperature and cross-flow velocity were selected as operating factors, while the initial flux decline rate, the final flux, and the final thickness of the fouling layer were selected as responses after a preliminary phase investigation of experimental results. The Supplementary Material appendix presents further details of the applied CCD method and analyses. The selected ranges of investigation for the various factors are reported in Table 2, together with the coded experimental values extrapolated by Design Expert software. The CCD method generated a suggestion for nine total runs, each with a specific combination of values of T_f and CFV. This procedure allowed weighted probing of the entire multidimensional space. The experimental results were used as input data to generate the model for each response according to the best fit. ANOVA was used for the statistical analysis of the results to evaluate the quality of the model.

Table 2. Experimental design of the selected of operating conditions, representing the range of experimental variables used in the RSM model

Factors	Unit	Minimum	Maximum	Coded low	Coded high	Mean
Temperature	(C°)	35.0	65.0	40.0	60.6	50.0
Cross-flow velocity	(m/s)	0.21	0.42	0.24	0.39	0.31

2.4 Filtration experiments protocol

Fouling experiments consisted of two phases: (i) a stable flux phase and (ii) a fouling phase. The flux was first stabilized using DI water only as feed, without organic foulants (J_0). This stage allowed achievement of the hydrodynamic equilibrium. The fouling phase then started at time zero, when the appropriate amount of organic foulant stock solution was added into the feed tank. This second phase was run until a volume concentration factor of 2.5 was reached, which was always associated with sufficient operational time to obtain a near stable flux and fouling layer thickness. The increment of $CaCl_2$ concentration during experiments can be considered negligible for any possible effect in the reduction of the feed vapor tension value. For this reason, the flux decrement observed during the fouling tests can be predominantly attributed to foulant deposition.

2.5 Optical coherence tomography (OCT) analysis

A spectral-domain optical coherence tomography (SD-OCT) system Ganymede II from Thorlabs, GmbH (Germany) was used to assess the fouling deposition on the membrane surface under accelerated fouling conditions. The OCT was equipped with a scan lens (LSM 03BB). The OCT probe was positioned on top of middle point of the DCMD module to characterize the fouling layer thickness at the end of each experiment. 3D cross-sectional OCT scans (666 pixel × 666 pixel × 1022 pixel) corresponded to 4.0 mm × 4.0 mm × 2.25 mm (width × length × depth). The OCT scans were processed with the FiJi software. Images were filtered to reduce the noise, then the contrast and brightness were adjusted. 3D scans were then visualized by AVIZO (Field Electron and Ion Company, Hillsboro, OR, USA) software and modified for visualization purpose. The fouling layer thickness was calculated using a customized MATLAB code.

3 Results and discussion

3.1 Beyond the RSM: An overall picture of the process parameters in MD organic fouling

3.1.1 The Effect of temperature and cross-flow velocity on the experimental flux

This section describes the experimental results while providing an in-depth understanding of the selected responses (dependent variables) of the RSM model. In this study, Design Expert was employed as a statistical tool to create the experiment plan aimed at studying the impact of operating condition on the fouling behavior in DCMD. The list of experiments is reported in Table S.1 and in the legend of Fig 1, where experimental results of water production in DCMD at different operating conditions are also shown.

In DCMD process, the initial flux, $J_{0,}$ is related to the feed temperature and cross-flow velocity [34, 35]. As expected, in this study the inlet feed temperature was found to govern J_0. By increasing T_f from 35 to 65 °C, the J_0 increased from 3 to 22.5 kg $m^{-2}h^{-1}$, while increasing the cross-flow velocity from 0.21 to 0.42 m/s at fixed T_f 50 °C led to an increase of only 2 kg $m^{-2}h^{-1}$. This result can be attributed to the nature of the driving force, namely, the vapor tension difference between the feed and the permeate, which can be easily determined through Antoine equation [36]. On the other hand, the cross-flow velocity can contribute to the flux increment by reducing the temperature polarization effects [37].

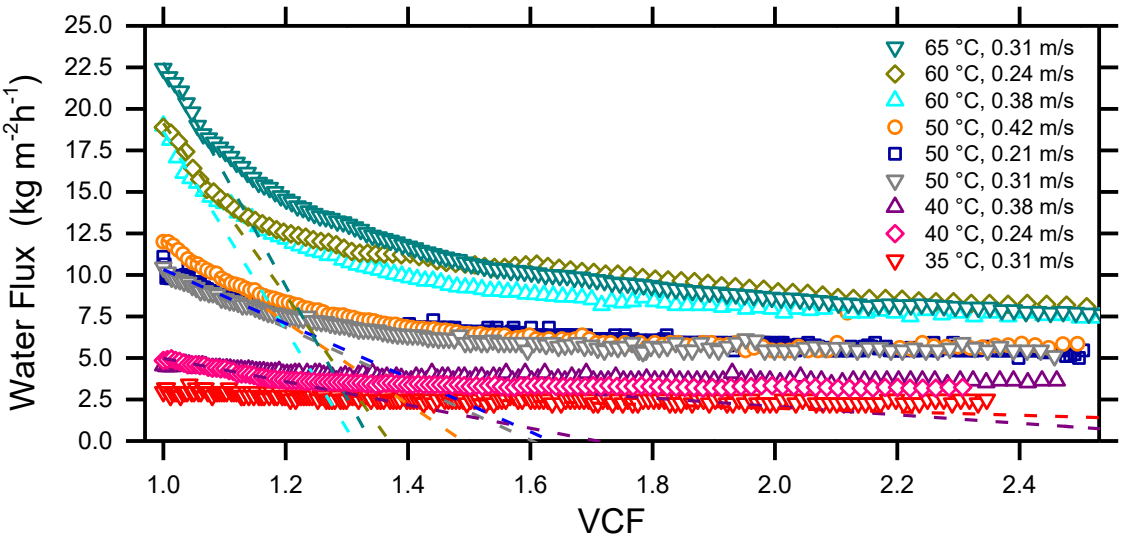

206

207 **Figure 1.** Results of fouling experiments performed with the synthetic feed water in the
208 presence of 500 mg/L humic acid and 20 mM of calcium chloride at different initial permeate
209 flux, J_0, obtained by changing the applied feed temperature and cross-flow velocity in DCMD.
210 Water fluxes (J_w) were investigated until a volume concentration factor (VCF) of 2.5 was
211 reached, at which a value of near-stable final flux was observed for all the experiments. Dash
212 lines represent the best linear fit of the first 1.25 volume concentration factor (VCF) of the initial
213 flux decline.

214

215 In all the tests, the water flux decreased almost linearly in the initial phase, to then reach an
216 approximate flux stabilization over time when the nominal driving force was counterbalanced by
217 resistances due to fouling accumulation to yield a constant effective driving force [38]. As
218 fouling deposition is proportional to the water transport across the membrane, high accumulation
219 typically occurs in the initial phases of operation, contributing to the formation of a cake layer
220 during this initial stage [39, 40]. The initial flux decline rates were estimated from the best linear

fit (see dash lines in Fig 1a) of the water flux measured between 1 and 1.25 VCF. The values are reported as a function of the initial flux J_0 (Fig 2a) and of the inlet feed temperature (Fig 2b). The results suggest a smooth and gradually incrementing correlation of the initial flux decline when increasing J_0. The proportional effect of J_0 on the initial flux decline has been also widely investigated in osmotically and pressure-driven membrane processes [41-43]. As expected, an analogous behavior was observed when looking at the data as a function of the inlet feed temperature (Fig 2b), as the driving force is closely related to this parameter. The data also allow assessment of the role of the cross-flow velocity, whose increment seems to slightly affect the initial flux decline, as an indirect effect of slightly larger values of J_0 observed when increasing CFV. The values of near stable flux at the end of the tests, J_w, and the ratio J_w / J_0 were also extrapolated from the flux decline data for each tested condition.

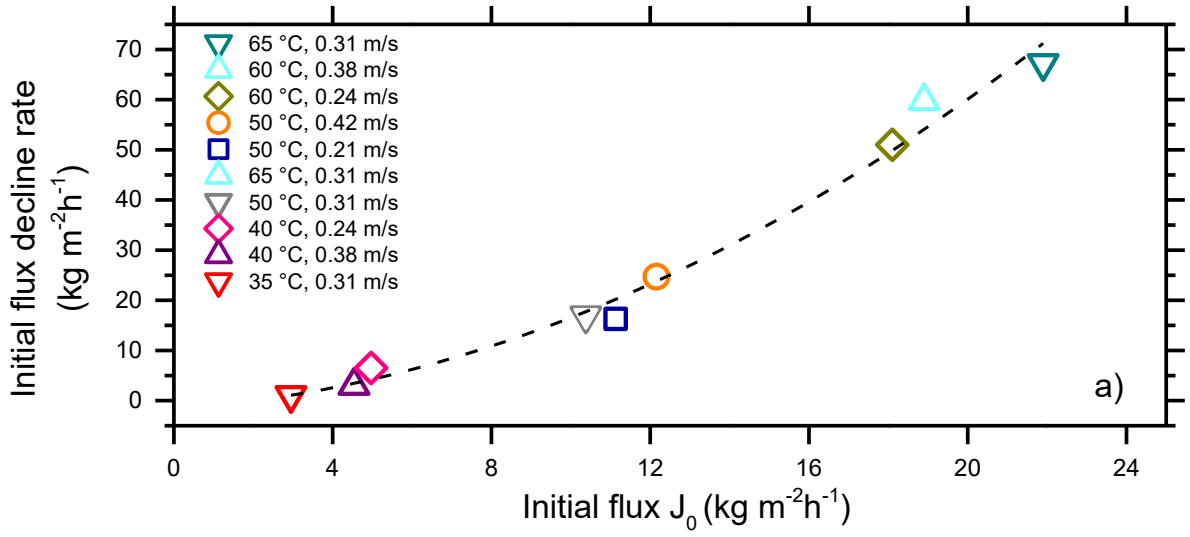

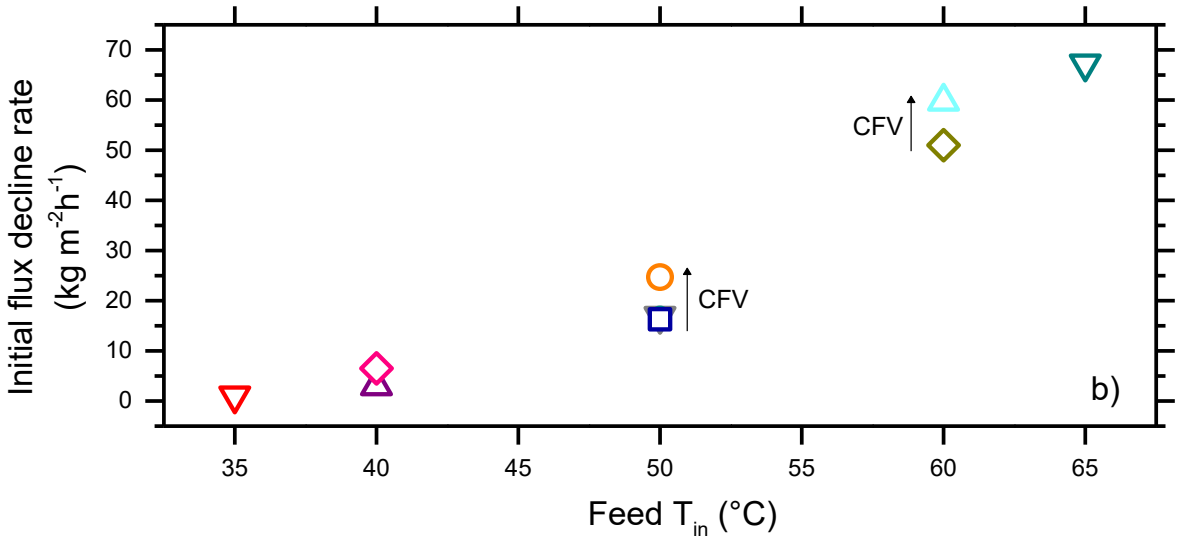

232 **Figure 2.** Plot of the initial flux decline rate as a function of (a) the initial permeate flux $J_{0,}$ and
233 (b) the inlet feed temperature (T_f). The arrows indicate the increment of the cross-flow velocity
234 (CFV). Data were extrapolated from dash lines rates reported in Fig 1.

235

236 A few interesting observations may be made by analyzing the data presented in Figs 1, 2. While
237 utilizing an inlet feed temperature set at 65 °C produced an initial flux (22.5 kg $m^{-2}h^{-1}$) that is
238 nine times higher the flux observed with a temperature equal to 35 °C (2.5 kg $m^{-2}h^{-1}$), the flux at
239 the end of the tests (J_w) was only 3 times larger, reaching roughly 7.5 kg $m^{-2}h^{-1}$ for the former
240 condition, whereas no significant decline in flux was observed at the lower feed temperature.
241 These results give reasons for operating at low-medium feed temperatures, namely, at or below
242 50 °C for water streams with high fouling potential and if membrane cleanings are not frequently
243 operated. In such cases, the long-term productivity may be similar within a wide range of bulk
244 feed temperature and working at lower temperature would result in savings in terms of energy
245 demand. This may in turn translate, e.g., into cheaper solar fields with smaller footprints if the

energy is harvested from the sun, or anyway into a higher energy efficiency and gain output ration (GOR) value for the overall process.

3.1.2 OCT results for the fouling layer thickness

Water flux data were linked to non-invasive direct fouling characterization performed with OCT to characterize the fouling layer developed on the membrane surface by scanning the central positions of the cell. Please note that the homogeneity of the fouling layer along the membrane length was confirmed by preliminarily evaluating the thickness growth at different positions of the cell. As no spatial gradient was observed, the middle position was selected as a representative location. The 3D OCT rendering images (Fig 3) show the fouling deposition obtained at T_f of 35, 50, 65 °C, thus covering the whole range of T_f investigated. The results highlight the increase of the foulant deposition by incrementing the inlet feed temperature. In these three examples, the same cross-flow velocity of 0.31 m/s was applied, representing the central point suggested by Design Expert within the explored CFV range (see Table S.1). In general, a slight increment of the foulant roughness was observed by increasing T_f, as nodule-like and valley-like structures became more pronounced. This phenomenon was also discussed by Laqbaqbi et al. when testing DCMD fouling at a temperature close to 70 °C [44].

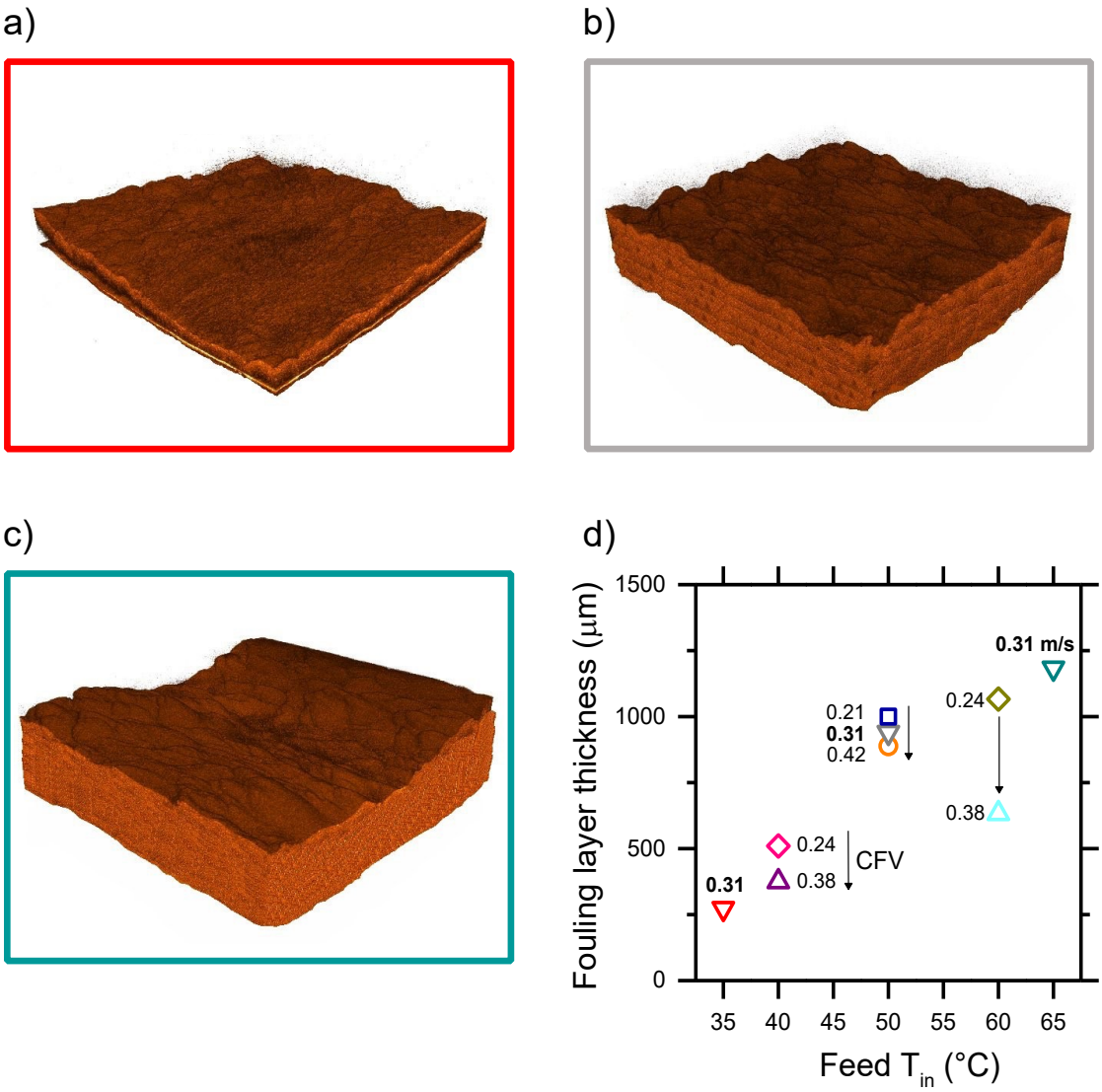

Figure 3. 3D OCT rendered scans (4mm × 4mm) of the final steady-state foulant layer thickness from the experiments conducted at cross-flow velocity of 0.31 m/s and feed inlet temperature of 35 °C, 50 °C, 65 °C in (a), (b), (c), respectively. The frame color of the OCT images corresponds to the color of the associated data points reported in (d). Here, the final thickness is plotted against the feed inlet temperature for all the tests. The number indicated close to each data point represents the cross-flow velocity associated with the respective test and expressed in m/s.

For all the experiments, fouling layer thickness measured with the OCT after 2.5 of volume concentration factor (VCF) is reported in Fig. 3d. In general, a near-linear increment of the thickness was observed as a function of T_f, for the entire investigated range of temperatures. Thus, the thickest deposition was observed for the experiment performed at 65 °C, achieving a layer thickness of almost 1200 µm at the end of the test. A much smaller layer of roughly 200 µm was observed with T_f of 35 °C. This last result is in agreement with previous DCMD studies reporting negligible organic fouling with a feed temperature below 40 °C [45]. As opposed to the effect of T_f, higher CFV values were beneficial for reducing the fouling layer development in MD. The arrows in Fig 3d indicate data points associated with different CFV values. As reported in the literature, the increment of the shear stress thwarted foulant accumulation by lowering the boundary layer thickness [46, 47].

The results presented imply a strong cause-consequence relation between the operating parameters in MD and fouling development, but without considering how fouling deposition can affect the overall driving force, i.e., the thermal balance during the process. Although the reciprocal influence between the driving force and fouling deposition has been widely investigated for pressure-driven and osmotically-driven processes [43, 48, 49], further research efforts are required to evaluate the interaction between governing factors and fouling in MD. In summary, the *in-situ* observation performed in this study confirmed the link between feed temperature and fouling propensity. The fouling thickness was found to (i) increase with feed inlet temperatures T_f, while (ii) slightly decreasing with cross-flow velocity. The thickness of the fouling layer may thus also be used as a robust response parameter for the RSM analysis discussed below.

3.2 Modeling of organic fouling in DCMD through response surface methodology (RSM)

3.2.1 Significance of operating parameters

Organic fouling in DCMD was investigated under different feed inlet temperatures and cross-flow velocities by performing nine DCMD filtration experiments, with combinations of operating parameters suggested by the central composite design approach. Based on the results described above, four parameters were selected as potentially valuable responses for the response surface analysis: (i) initial flux decline rate, (ii) J_w / J_0 value at the end of the test indicating the relative loss of productivity due to fouling, (iii) near-stable flux, (iv) final foulant layer thickness. Experimental results for these parameters were used as input data (responses) to generate the relative model function. According to Design Expert, all these responses were statistically significant to both T_f and CFV, i.e., low p-value. Table 3 summarizes the p-values obtained from ANOVA. Specifically, T_f was found to be considerably more significant than CFV. Each response was fitted by a different model function. The initial flux decline was described by a quadratic model while all the other responses were adequately described by a linear model, as can be seen by the absence of cross-correlation terms in Table 3. Within the three linear responses, CFV was not highly significant, as the p-value was > 0.1. However, CFV was included in the model to respect the hierarchy of the statistical method and to improve the fit [50]. For each response, the final equation calculated by Design Expert and relating operating parameters with fouling outcomes (responses) is reported in the Supplementary Material appendix (see Table S.2.).

Table 3 Summary of response significance values estimated by ANOVA statistical analysis.

Source	Initial flux decline p-value	Final J_w/J_0 p-value	Final flux p-value	Final thickness p-value

Model	0.0001	0.0004	< 0.0001	0.0133
A-Cross-flow velocity	0.0835	0.4156	0.2145	0.2191
B-Feed temperature	< 0.0001	0.0001	< 0.0001	0.0059
AB	0.0812			
A^2	0.1153			
B^2	0.0017			

315

316 To provide a detailed statistical analysis, the diagnostic plots of the initial flux decline, the final
317 flux, and the final J_w/J_0 values are shown in Fig S.2, S.3 and S.4, respectively. Figure 4 displays
318 the diagnostic plots for the final foulant layer thickness. Please note that the following discussion
319 relates directly to layer thickness, but the conclusions and implications are also valid for the
320 other selected responses. Figure 4a reports the normal probability plot of residuals (error terms),
321 a graphical tool for comparing a data set with the normal distribution: if the data can be
322 adequately described with a normal distribution, characterized by a mean and a variance, then a
323 plot of the theoretical percentiles of the normal distribution versus the observed sample
324 percentiles should be approximately linear. In Fig 4a, the red linear line represents the theoretical
325 normal distribution while the ten dots represent the observed samples (10 runs, Table S1). For all
326 the responses, normal probability plot of the residuals fell on a straight line, which implies that
327 error terms had a normal distribution [51, 52].

328 Figure 4b shows that all points are scattered around the 0 y-axis (variance or standard deviation)
329 reflecting equal or similar variances of collected data. In fact, nine points out of ten lie within
330 two standard deviations, meaning that 95% of values are included in this range (empirical rule).
331 In this case, the variance of residuals can be considered as a constant (homoscedasticity).
332 Homoscedasticity is an important assumption of parametric statistical tests. In Fig. 4c, residuals
333 vs. data points do not follow a specific pattern, which suggests that responses are not dependent
334 on the order of runs. Lastly, Fig. 4d illustrates that predicted values vs. experimental values lay

on a straight 45 degree line, an indication of high-quality modeling outcome. In conclusion, the diagnostic plots of all the responses indicate the robustness of the statistical analysis, which enable to assess the impact of the operating parameters on the organic fouling behavior in MD.

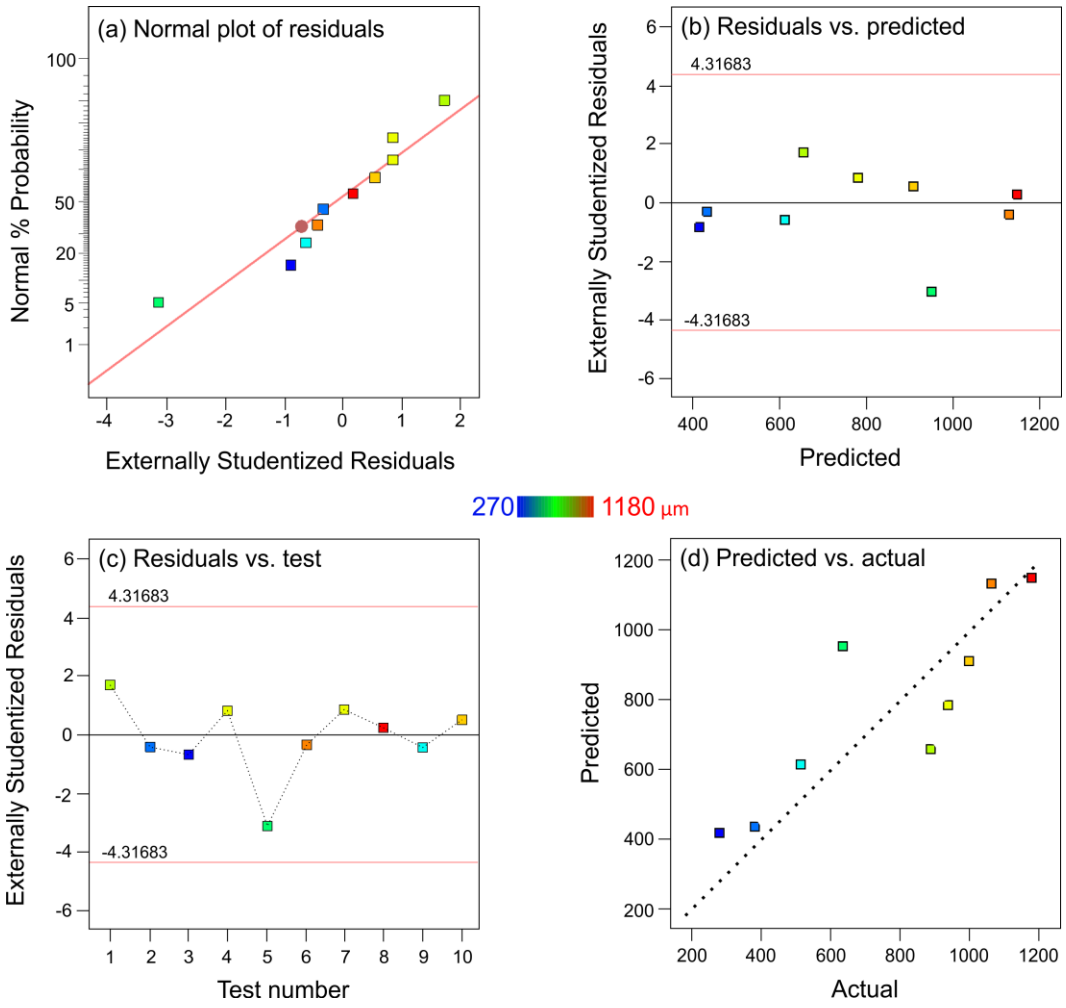

Figure 4. Diagnostic plots for the foulant layer thickness response: (a) normal % probability vs. residuals; (b) residuals vs. predicted; (c) residuals vs. run order; (d) predicted vs. actual.

3.2.2 Single responses evaluation

Fig 5 shows the outcome of the RSM model in terms of effects of operating parameters, i.e., temperature and cross-flow velocity, on the fouling behavior, namely, initial flux decline rate, final J_w/J_0, the near-stable flux, and the final layer thickness. This discussion aims at providing an effective view of fouling behavior in the whole range of investigated conditions of T_f and CFV and to facilitate any direct comparison among the selected fouling parameters. In accordance with the description in the section above, all the responses were mainly governed by the feed temperature. Specifically, Fig 5b shows how contour values decrease from a J_w / J_0 of 0.7 to below 0.3 when the T_f increases from 40 to 65 °C, thus only roughly 1 kg $m^{-2}h^{-1}$ of stable flux is gained for each 5 °C-step in ΔT_f (see Fig 5c). As illustrated in Fig 5c, a net increment of the fouling deposition can be observed by increasing T_f, as a twofold increase of layer thickness is associated to an increase of the temperature from 40 to 65 °C.

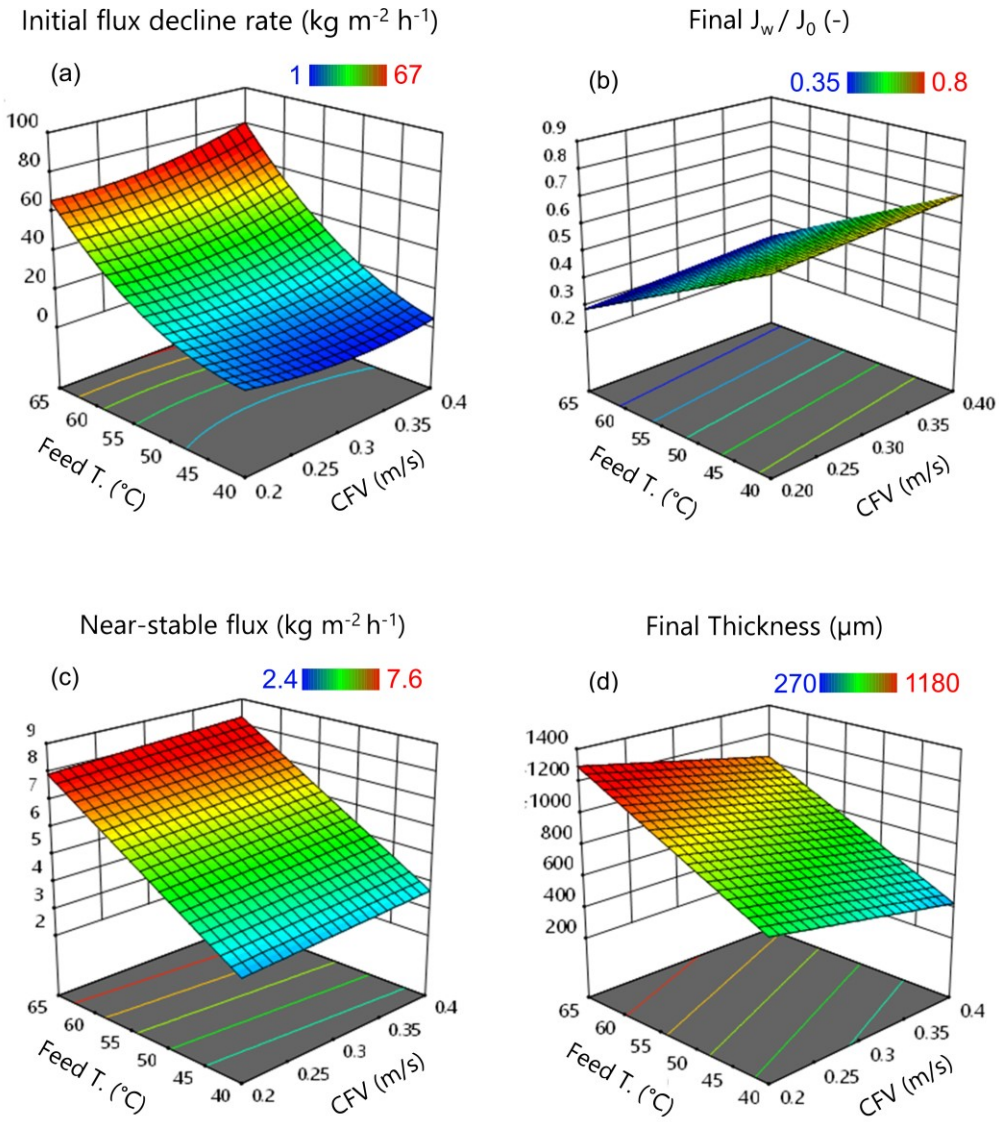

Figure 5. 2D surface response plots as a function of the feed inlet temperature and cross-flow velocity for the (a) initial flux decline rate, (b) final to initial flux ration, (c) near-stable flux, and (d) final foulant layer thickness. The near-stable flux is the flux at volume concentration factor of 2.5 for the experiments reported in Fig 1. The magnitude for each response increases from blue to red and is also indicated by numeric values for each contour line.

In contrast to feed inlet temperature, different behaviors were observed by varying the cross-flow velocity. The initial flux decline rate was more affected by the CFV at higher T_f values (see Fig 5a). This result can be explained by the proportionality between T_f and temperature polarization (TP) [52]. Faster CFVs thwart TP and this effect is more pronounced when TP tends to be of greater magnitude, that is, at higher values of T_f. This translates into larger J_0 (see Fig 1) and the ensuing steeper flux decline, as observed for CFV values above 0.3 m/s [53, 54]. On the other hand, increasing CFV yielded a positive outcome in terms of productivity when considering the magnitude of the near-stable flux (see Fig 5b, c), likely due to lower fouling deposition associated with smaller boundary layers, as observed in Fig 5c. In fact, the OCT scans highlighted a reduction in fouling layer thickness by increasing the CFV. Interestingly, the CFV was more impactful in decreasing the foulant thickness rather than increasing the overall flux decline J_w / J_0, implying that foulant thickness and flux loss are not directly correlated but that a complex mechanism is in play. This result might be rationalized with the fact that these two parameters are not independent, for example, J_w may not simply intensify the likelihood of foulant deposition but simultaneously cause enhanced compactness of the resulting layer [55]. Both thickness and compactness of the foulant layer play a role in mass and heat transport, and thicker but more porous layer may be less detrimental than thin dense layers that would produce a larger variation in diffusion coefficients and thermal conductivity with respect to the bulk solution.

In conclusion, the RSM analysis well depicted the link between fouling propensity and feed temperature, as fouling behavior worsened with the increase of the feed inlet temperature, thereby negatively affecting the flux decline, J_w/J_0, while a positive but gradually more marginal enhancement of productivity (near-stable flux) was observed when increasing the feed inlet

384 temperature. Moreover, it was found that the increase in cross-flow velocity led to a slight
385 decrease of the fouling thickness deposited on the membrane, while keeping an overall benefit in
386 terms of productivity.

Conclusions

Organic fouling in MD process was investigated using humic acid and calcium chloride in the feed solution. The goal of this study was to assess the role of the feed temperature and cross-flow velocity on fouling behaviour in DCMD. The different operating conditions of the experiments were selected through Design Expert software aiming to build the model function of the selected responses. The four process performance parameters selected as responses (dependent variables) for the RSM were: (i) the initial flux decline rate, (ii) the near-stable flux measured at the end of the tests, (iii) the stable to initial flux ration, J_w / J_0, and (iv) the final fouling layer thickness.

Higher influence of feed inlet temperature than cross-flow velocity on loss of productivity was observed experimentally and then confirmed by robust statistical analysis, due to the major role of flux in the development of organic fouling in DCMD. In detail, a sharp increment in the overall flux decline, J_w/J_0 occurred at higher feed inlet temperatures, making the case for the need to select an appropriately transmembrane temperature difference that guarantees feasible fluxes but also minimizes loss of driving force and energy demand. The benefits in water productivity obtained by increasing the feed temperature were always offset by higher fouling deposition.

Another interesting trade-off between more rapid initial flux decline and thinner layer thickness was observed by increasing cross-flow velocity above 0.3 m/s. Layer thickness is only one of many aspects of the foulant layer that relates to productivity loss, others may include density, pore structure and thermal conductivity, which can directly influence mass and heat transport through this unmixed layer. Optical coherence tomography (OCT) was used in this study to assess layer thickness, but further efforts are needed to deepen investigations

410 on foulant deposition and on how layer characteristics relate to deposition mode and then
411 flux loss. Overall, working at relatively high cross-flow velocity may be beneficial at high
412 values of the nominal driving force, i.e., transmembrane temperature difference, while the
413 results suggest that the effect of channel feed flow velocity may not play a significant role
414 when the flux is below a certain level, approximately 10 kg $m^{-2}h^{-1}$.

415 Finally, the proposed approach is not limited to this application but was proven to be a valuable
416 tool to assess the role of the process parameters and governing factors on fouling and process
417 performance in membrane distillation (MD). The results of this study highlight the effectiveness
418 of combining flux data, OCT characterization, and response surface methodology (RSM) to
419 advance the understanding of fouling in MD and open future perspective related to this crucial
420 topic to making MD feasible at commercial scale.

Supplementary material

Assessing the effect of feed temperature and cross-flow velocity on organic fouling in membrane distillation using response surface methodology

Francesco Ricceri[a], Bastiaan Blankert [b], Johannes S. Vrouwenvelder[b], Alberto Tiraferri[a]*, Luca Fortunato[b]*

[a] Department of Environment, Land and Infrastructure Engineering (DIATI), Politecnico di Torino, Corso Duca degli Abruzzi 24, Turin, 10129, Italy

[b] Water Desalination and Reuse Center (WDRC), King Abdullah University of Science and Technology (KAUST), Biological & Environmental Science & Engineering Division (BESE), Thuwal 23955-6900, Saudi Arabia

* Corresponding authors

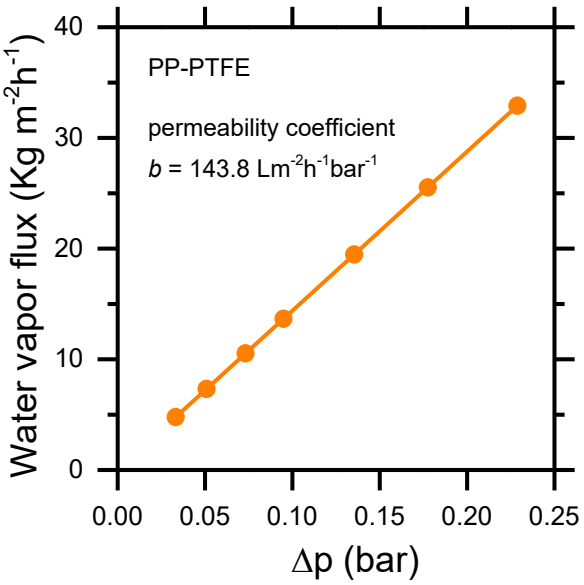

435

436 **Figure S.1.** Linear correlation between the obtained water vapor flux as a function of the
437 applied vapor tension difference for the PP-PTFE membrane. The permeability, *b*, is
438 reported.

439

440 **Table S.1.** List of the experiments suggested by Design Expert software for different
441 combinations of cross-flow velocity and inlet feed temperature. Related experimental results
442 for each response are also listed from the third column. C.P indicates the central point, a
443 repetition of the 4th run, required by the software to retrieve a better model fitting.

Run	CFV	T_f	Initial flux decline	Final flux	Final thickness	J_w/J_0
-	m/s	°C	Kg m^{-2} h^{-1}/[-]	Kg m^{-2} h^{-1}	µm	-
1	0.42	50.0	24.7	5.8	888	0.48
2	0.39	39.4	3.0	3.6	375	0.79
3	0.31	35.0	1.1	2.4	273	0.80
4	0.31	50.0	16.9	5.4	940	0.52
5	0.39	60.6	59.7	7.4	633	0.39
6	0.24	60.6	51.0	7.6	1066	0.42
7	0.31	65.0	67.2	7.6	1183	0.34
8	0.24	39.4	6.5	3.2	510	0.64
9	0.21	50.0	16.3	5.2	1000	0.47
C.P	0.31	50.0	17.6	5.1	920	0.57

444

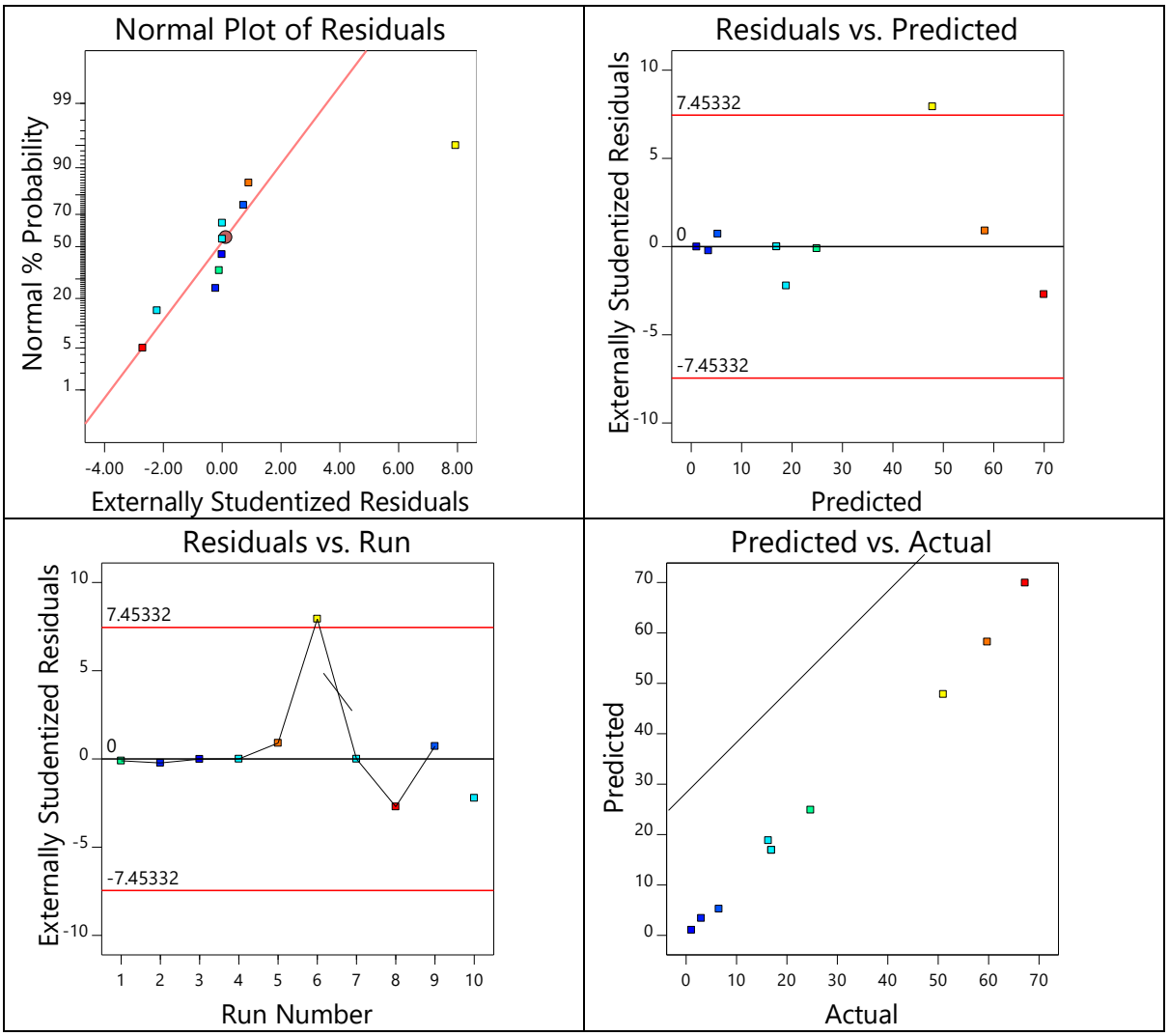

Figure S.2. Diagnostic plots for initial flux decline rate as response: (a) normal % probability vs. residuals; (b) residuals vs. predicted; (c) residuals vs. run order; (d) predicted vs. actual.

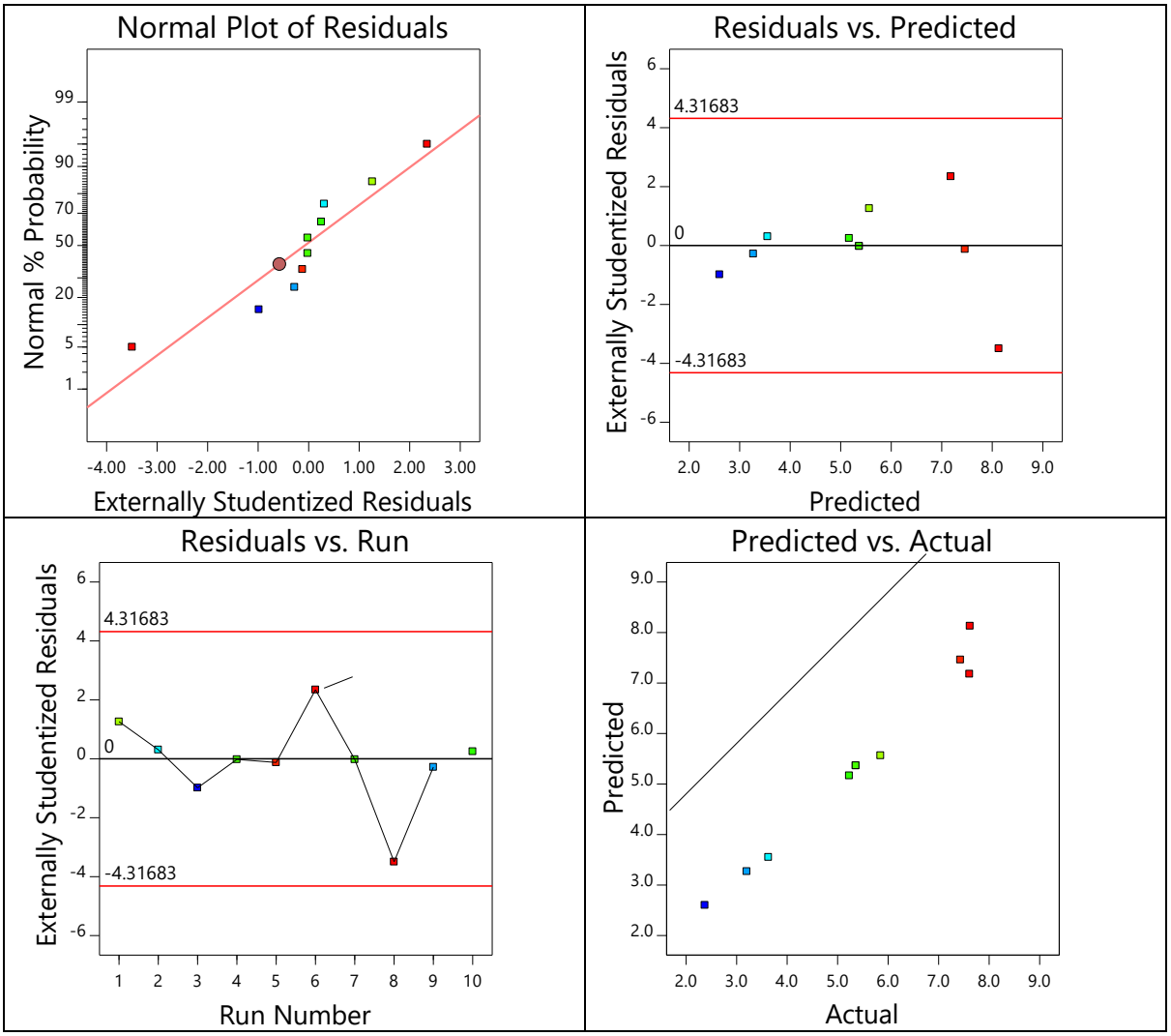

Figure S.3. Diagnostic plots for near-stable flux at the end of the test as response: (a) normal % probability vs. residuals; (b) residuals vs. predicted; (c) residuals vs. run order; (d) predicted vs. actual.

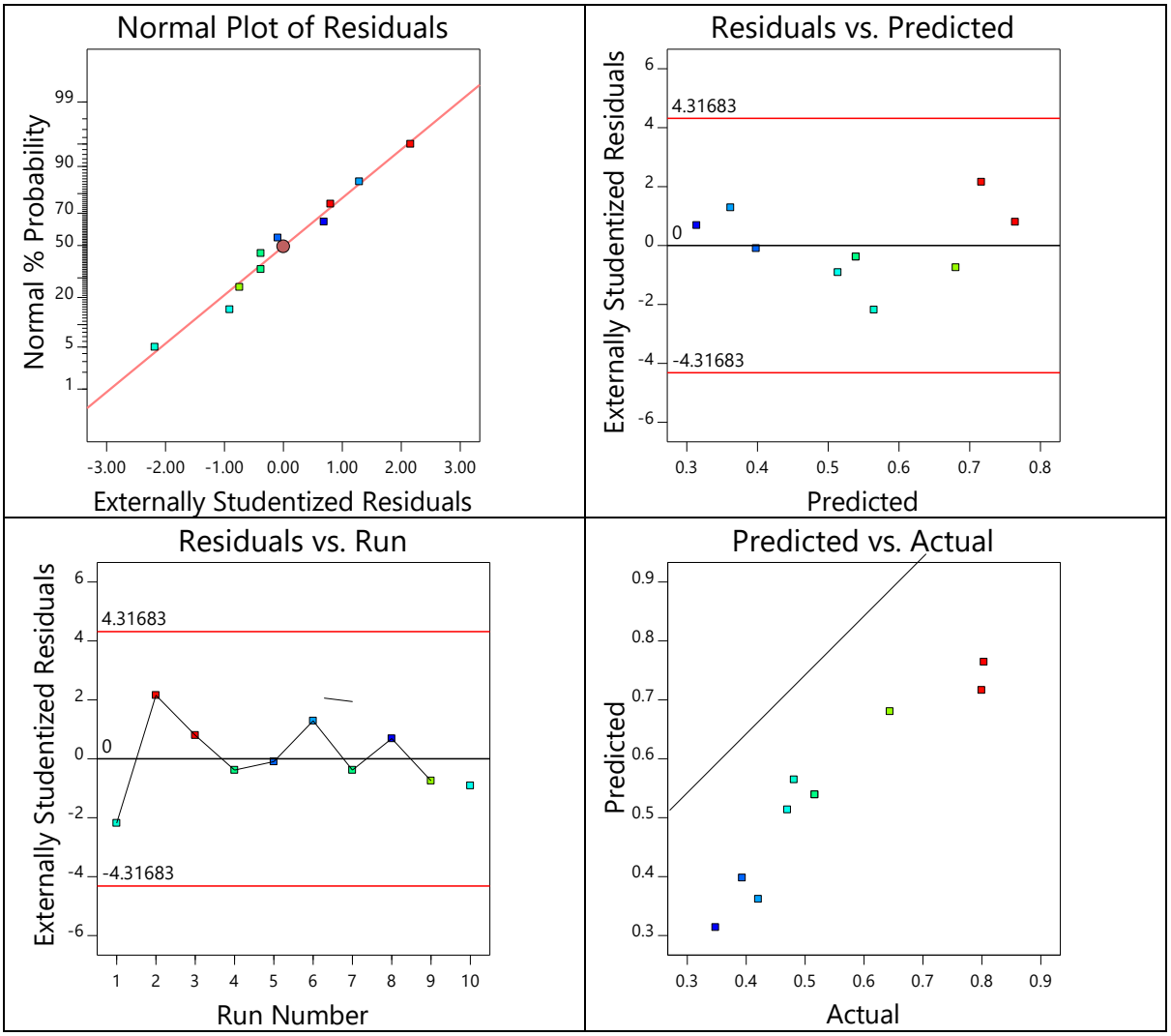

456

457 **Figure S.4.** Diagnostic plots for J_w/J_0 as response: (a) normal % probability vs. residuals; (b)

458 residuals vs. predicted; (c) residuals vs. run order; (d) predicted vs. actual.

459

460 **Tab S.2.** Final equations computed by the statistical analysis and relating operating

461 parameters to fouling behaviour. The equation can be used to make predictions about each

462 response.

		Initial Flux decline	Final Flux	Final Thickness	J_w/J_0
		+206.19420	+5.37	+780.80	+1.21292
A-Cross flow velocity	*	-452.03539	+0.1409	-90.80	+0.243943
B-Feed temperature	*	-7.19720	+1.95	+262.62	-0.015014
AB	*	+3.90112			

A^2	*	+453.12607			
B^2	*	+0.082623			

Appendix

The model is generated for the four responses and is based on experimental data collected in the lab fitting a linear model for the final flux, final thickness, and final J_w/J_0 responses and a fitting a quadratic model for the initial flux decline rate response. The most general equation is reported here below:

$$y = \beta_0 + \sum k_i = 1 \beta_i x_i + \sum k_i = 1 \beta_{ii} x_i^2 + \sum k_i = 1 \sum k_j = i + 1 \beta_{ij} x_i x_j + \varepsilon \quad \text{(Eq S.2)}$$

where y is the predicted response, x represents the factors, k is the number of factors, β_0 is the constant coefficient, and β_i, β_{ii}, and β_{ij} are the regression coefficients of linear, quadratic, and interaction terms, respectively. To select the amount of experimental data to be collected, Central Composite Design (CCD) was applied. This design defines 2k corner points, 2k axial points, where k is the number of independent variables (or factors) selected, and a central point. In this study, two factors (Feed inlet temperature and feed cross-flow velocity) were selected. The number of experiments was directly calculated by the software according to the equation $n = 2^k \cdot 2k + Cp$, resulting in a total of 10 experiments, one of them represented by the central point (Cp). These test are a combination of different factors levels defined by the coded values calculated by applying the formulas in Table S2. The coded value associated with α is representative of the rotatability of the model which suggested Practical alpha due to $k < 6$ and equal to 1,41, which represents the distance.

Table S2. Coded and un-coded values for CCD

Coded value	Un-coded value
-α	X_{min}
-1	$\frac{(\alpha-1)X_{max}+(\alpha+1)X_{min}}{2\alpha}$
0	$\frac{X_{max}+X_{min}}{2}$
+1	$\frac{(\alpha-1)X_{min}+(\alpha+1)X_{max}}{2\alpha}$
+α	X_{max}

485

References

[1] N. Thomas, M.O. Mavukkandy, S. Loutatidou, H.A. Arafat, Membrane distillation research & implementation: Lessons from the past five decades, Separation and Purification Technology, 189 (2017) 108-127.

[2] L.M. Camacho, L. Dumée, J. Zhang, J.-d. Li, M. Duke, J. Gomez, S. Gray, Advances in membrane distillation for water desalination and purification applications, Water, 5 (2013) 94-196.

[3] I. Hitsov, L. Eykens, W. De Schepper, K. De Sitter, C. Dotremont, I. Nopens, Full-scale direct contact membrane distillation (DCMD) model including membrane compaction effects, Journal of membrane science, 524 (2017) 245-256.

[4] G. Dong, J.F. Kim, J.H. Kim, E. Drioli, Y.M. Lee, Open-source predictive simulators for scale-up of direct contact membrane distillation modules for seawater desalination, Desalination, 402 (2017) 72-87.

[5] H. Susanto, Towards practical implementations of membrane distillation, Chemical Engineering and Processing: Process Intensification, 50 (2011) 139-150.

[6] M. Khayet, T. Matsuura, Membrane distillation: principles and applications, (2011).

[7] B. Ashoor, S. Mansour, A. Giwa, V. Dufour, S. Hasan, Principles and applications of direct contact membrane distillation (DCMD): a comprehensive review, Desalination, 398 (2016) 222-246.

[8] T. Horseman, Y. Yin, K.S. Christie, Z. Wang, T. Tong, S. Lin, Wetting, scaling, and fouling in membrane distillation: State-of-the-art insights on fundamental mechanisms and mitigation strategies, ACS ES&T Engineering, 1 (2020) 117-140.

[9] M. Rezaei, D.M. Warsinger, M.C. Duke, T. Matsuura, W.M. Samhaber, Wetting phenomena in membrane distillation: Mechanisms, reversal, and prevention, Water research, 139 (2018) 329-352.

[10] E. Guillen-Burrieza, M. Mavukkandy, M. Bilad, H. Arafat, Understanding wetting phenomena in membrane distillation and how operational parameters can affect it, Journal of Membrane Science, 515 (2016) 163-174.

[11] S. Shao, D. Shi, J. Hu, W. Qing, X. Li, X. Li, B. Ji, Z. Yang, H. Guo, C.Y. Tang, Unraveling the Kinetics and Mechanism of Surfactant-Induced Wetting in Membrane Distillation: An In Situ Observation with Optical Coherence Tomography, Environmental science & technology, (2021).

[12] D. Hou, Z. Yuan, M. Tang, K. Wang, J. Wang, Effect and mechanism of an anionic surfactant on membrane performance during direct contact membrane distillation, Journal of Membrane Science, 595 (2020) 117495.

[13] K.S. Christie, Y. Yin, S. Lin, T. Tong, Distinct behaviors between gypsum and silica scaling in membrane distillation, Environmental science & technology, 54 (2019) 568-576.

[14] M. Gryta, Fouling in direct contact membrane distillation process, Journal of membrane science, 325 (2008) 383-394.

[15] P. Wang, T.-S. Chung, Recent advances in membrane distillation processes: Membrane development, configuration design and application exploring, Journal of membrane science, 474 (2015) 39-56.

[16] F. Ricceri, M. Giagnorio, G. Farinelli, G. Blandini, M. Minella, D. Vione, A. Tiraferri, Desalination of produced Water by Membrane Distillation: Effect of the feed components and of a pre-treatment by fenton oxidation, Scientific reports, 9 (2019) 1-12.

[17] L. Fortunato, H. Elcik, B. Blankert, N. Ghaffour, J. Vrouwenvelder, Textile dye wastewater treatment by direct contact membrane distillation: Membrane performance and detailed fouling analysis, Journal of Membrane Science, 636 (2021) 119552.

[18] J. Guo, L. Fortunato, B.J. Deka, S. Jeong, A.K. An, Elucidating the fouling mechanism in pharmaceutical wastewater treatment by membrane distillation, Desalination, 475 (2020) 114148.

[19] J.-G. Lee, Y. Jang, L. Fortunato, S. Jeong, S. Lee, T. Leiknes, N. Ghaffour, An advanced online monitoring approach to study the scaling behavior in direct contact membrane distillation, Journal of Membrane Science, 546 (2018) 50-60.

[20] A. Abdel-Karim, S. Leaper, C. Skuse, G. Zaragoza, M. Gryta, P. Gorgojo, Membrane cleaning and pretreatments in membrane distillation-a review, Chemical Engineering Journal, (2021) 129696.
[21] C.A. Robbins, Y. Yin, A.J. Hanson, J. Blotevogel, T. Borch, T. Tong, Mitigating membrane wetting in the treatment of unconventional oil and gas wastewater by membrane distillation: A comparison of pretreatment with omniphobic membrane, Journal of Membrane Science, (2021) 120198.
[22] G. Naidu, S. Jeong, S.-J. Kim, I.S. Kim, S. Vigneswaran, Organic fouling behavior in direct contact membrane distillation, Desalination, 347 (2014) 230-239.
[23] F. Wendland, A. Blum, M. Coetsiers, R. Gorova, J. Griffioen, J. Grima, K. Hinsby, R. Kunkel, A. Marandi, T. Melo, European aquifer typology: a practical framework for an overview of major groundwater composition at European scale, Environmental Geology, 55 (2008) 77-85.
[24] R. Valladares Linares, L. Fortunato, N. Farhat, S. Bucs, M. Staal, E. Fridjonsson, M. Johns, J.S. Vrouwenvelder, T. Leiknes, Mini-review: novel non-destructive in situ biofilm characterization techniques in membrane systems, Desalination and Water Treatment, 57 (2016) 22894-22901.
[25] L. Fortunato, A.F. Lamprea, T. Leiknes, Evaluation of membrane fouling mitigation strategies in an algal membrane photobioreactor (AMPBR) treating secondary wastewater effluent, Science of The Total Environment, 708 (2020) 134548.
[26] L. Fortunato, Y. Jang, J.-G. Lee, S. Jeong, S. Lee, T. Leiknes, N. Ghaffour, Fouling development in direct contact membrane distillation: Non-invasive monitoring and destructive analysis, Water research, 132 (2018) 34-41.
[27] F. Ricceri, G. Farinelli, M. Giagnorio, A. Zamboi, A. Tiraferri, Optimization of physico-chemical and membrane filtration processes to remove high molecular weight polymers from produced water in enhanced oil recovery operations, Journal of Environmental Management, 302 (2022) 114015.
[28] I. Righetto, R.A. Al-Juboori, J.U. Kaljunen, A. Mikola, Multipurpose treatment of landfill leachate using natural coagulants–Pretreatment for nutrient recovery and removal of heavy metals and micropollutants, Journal of Environmental Chemical Engineering, 9 (2021) 105213.
[29] I. Righetto, R.A. Al-Juboori, J.U. Kaljunen, A. Mikola, Wastewater treatment with starch-based coagulants for nutrient recovery purposes: Testing on lab and pilot scales, Journal of Environmental Management, 284 (2021) 112021.
[30] M. Ahmadi, F. Vahabzadeh, B. Bonakdarpour, E. Mofarrah, M. Mehranian, Application of the central composite design and response surface methodology to the advanced treatment of olive oil processing wastewater using Fenton's peroxidation, Journal of Hazardous Materials, 123 (2005) 187-195.
[31] T. Rakić, I. Kasagić-Vujanović, M. Jovanović, B. Jančić-Stojanović, D. Ivanović, Comparison of full factorial design, central composite design, and box-behnken design in chromatographic method development for the determination of fluconazole and its impurities, Analytical Letters, 47 (2014) 1334-1347.
[32] M. Shokrollahi, M. Rezakazemi, M. Younas, Producing water from saline streams using membrane distillation: modeling and optimization using CFD and design expert, International Journal of Energy Research, 44 (2020) 8841-8853.
[33] S. Srisurichan, R. Jiraratananon, A. Fane, Humic acid fouling in the membrane distillation process, Desalination, 174 (2005) 63-72.
[34] G. Naidu, S. Jeong, S. Vigneswaran, Influence of feed/permeate velocity on scaling development in a direct contact membrane distillation, Separation and Purification Technology, 125 (2014) 291-300.
[35] S. Al-Obaidani, E. Curcio, F. Macedonio, G. Di Profio, H. Al-Hinai, E. Drioli, Potential of membrane distillation in seawater desalination: thermal efficiency, sensitivity study and cost estimation, Journal of membrane science, 323 (2008) 85-98.
[36] F.A. Banat, J. Simandl, Theoretical and experimental study in membrane distillation, Desalination, 95 (1994) 39-52.
[37] G.W. Thomson, The Antoine equation for vapor-pressure data, Chemical reviews, 38 (1946) 1-39.

[38] C. Boo, S. Hong, M. Elimelech, Relating organic fouling in membrane distillation to intermolecular adhesion forces and interfacial surface energies, Environmental science & technology, 52 (2018) 14198-14207.
[39] A. Alkhatib, M.A. Ayari, A.H. Hawari, Fouling mitigation strategies for different foulants in membrane distillation, Chemical Engineering and Processing-Process Intensification, 167 (2021) 108517.
[40] A. Hausmann, P. Sanciolo, T. Vasiljevic, M. Weeks, K. Schroën, S. Gray, M. Duke, Fouling mechanisms of dairy streams during membrane distillation, Journal of Membrane Science, 441 (2013) 102-111.
[41] R.W. Field, G.K. Pearce, Critical, sustainable and threshold fluxes for membrane filtration with water industry applications, Advances in colloid and interface science, 164 (2011) 38-44.
[42] T.-T. Nguyen, C. Lee, R.W. Field, I.S. Kim, Insight into organic fouling behavior in polyamide thin-film composite forward osmosis membrane: Critical flux and its impact on the economics of water reclamation, Journal of Membrane Science, 606 (2020) 118118.
[43] F. Ricceri, M. Giagnorio, K.R. Zodrow, A. Tiraferri, Organic fouling in forward osmosis: Governing factors and a direct comparison with membrane filtration driven by hydraulic pressure, Journal of Membrane Science, 619 (2021) 118759.
[44] M. Laqbaqbi, M. García-Payo, M. Khayet, J. El Kharraz, M. Chaouch, Application of direct contact membrane distillation for textile wastewater treatment and fouling study, Separation and Purification Technology, 209 (2019) 815-825.
[45] J. Ortiz de Zárate, C. Rincón, J. Mengual, Concentration of bovine serum albumin aqueous solutions by membrane distillation, Separation science and technology, 33 (1998) 283-296.
[46] S. Srisurichan, R. Jiraratananon, A. Fane, Mass transfer mechanisms and transport resistances in direct contact membrane distillation process, Journal of membrane science, 277 (2006) 186-194.
[47] L. Eykens, I. Hitsov, K. De Sitter, C. Dotremont, L. Pinoy, I. Nopens, B. Van der Bruggen, Influence of membrane thickness and process conditions on direct contact membrane distillation at different salinities, Journal of Membrane Science, 498 (2016) 353-364.
[48] M.S. Toran, A. D'Haese, I. Rodríguez-Roda, W. Gernjak, Fouling propensity of novel TFC membranes with different osmotic and hydraulic pressure driving forces, Water Research, 175 (2020) 115657.
[49] F.A. Siddiqui, Q. She, A.G. Fane, R.W. Field, Exploring the differences between forward osmosis and reverse osmosis fouling, Journal of Membrane Science, 565 (2018) 241-253.
[50] N. Biglarijoo, S.A. Mirbagheri, M. Ehteshami, S.M. Ghaznavi, Optimization of Fenton process using response surface methodology and analytic hierarchy process for landfill leachate treatment, Process Safety and Environmental Protection, 104 (2016) 150-160.
[51] H. Pashaei, A. Ghaemi, M. Nasiri, B. Karami, Experimental modeling and optimization of CO2 absorption into piperazine solutions using RSM-CCD methodology, ACS omega, 5 (2020) 8432-8448.
[52] M. Qtaishat, T. Matsuura, B. Kruczek, M. Khayet, Heat and mass transfer analysis in direct contact membrane distillation, Desalination, 219 (2008) 272-292.
[53] Z. Ding, L. Liu, Z. Liu, R. Ma, Fouling resistance in concentrating TCM extract by direct contact membrane distillation, Journal of Membrane Science, 362 (2010) 317-325.
[54] A. Hausmann, P. Sanciolo, T. Vasiljevic, U. Kulozik, M. Duke, Performance assessment of membrane distillation for skim milk and whey processing, Journal of Dairy Science, 97 (2014) 56-71.
[55] M. Laqbaqbi, J.A. Sanmartino, M. Khayet, C. García-Payo, M. Chaouch, Fouling in membrane distillation, osmotic distillation and osmotic membrane distillation, Applied Sciences, 7 (2017) 334.